

Zwicky Transient Facility and Globular Clusters: The Period-Luminosity and Period-Wesenheit Relations for Type II Cepheids

CHOW-CHOONG NGEOW,¹ ANUPAM BHARDWAJ,² JING-YI HENDERSON,¹ MATTHEW J. GRAHAM,³ RUSS R. LAHER,⁴
MICHAEL S. MEDFORD,^{5,6} JOSIAH PURDUM,⁷ AND BEN RUSHOLME⁴

¹Graduate Institute of Astronomy, National Central University, 300 Zhongda Road, 32001 Zhongli, Taiwan

²INAF-Osservatorio astronomico di Capodimonte, Via Moiariello 16, 80131 Napoli, Italy

³Division of Physics, Mathematics, and Astronomy, California Institute of Technology, Pasadena, CA 91125, USA

⁴IPAC, California Institute of Technology, 1200 E. California Blvd, Pasadena, CA 91125, USA

⁵University of California, Berkeley, Department of Astronomy, Berkeley, CA 94720, USA

⁶Lawrence Berkeley National Laboratory, 1 Cyclotron Rd., Berkeley, CA 94720, USA

⁷Caltech Optical Observatories, California Institute of Technology, Pasadena, CA 91125, USA

ABSTRACT

We present the first *gri*-band period-luminosity (PL) and period-Wesenheit (PW) relations for 37 Type II Cepheids (hereafter TIIC) located in 18 globular clusters based on photometric data from the Zwicky Transient Facility. We also updated *BVIJHK*-band absolute magnitudes for 58 TIIC in 24 globular clusters using the latest homogeneous distances to the globular clusters. The slopes of *g/r/i* and *B/V/I* band PL relations are found to be statistically consistent when using the same sample of distance and reddening. We employed the calibration of *ri*-band PL/PW relations in globular clusters to estimate a distance to M31 based on a sample of ~ 270 TIIC from the PAndromeda project. The distance modulus to M31, obtained using calibrated *ri*-band PW relation, agrees well with the recent determination based on classical Cepheids. However, distance moduli derived using the calibrated *r*- and *i*-band PL relations are systematically smaller by ~ 0.2 mag, suggesting there are possible additional systematic error on the PL relations. Finally, we also derive the period-color (PC) relations and for the first time the period-Q-index (PQ) relations, where the *Q*-index is reddening-free, for our sample of TIIC. The PC relations based on $(r - i)$ and near-infrared colors and the PQ relations are found to be relatively independent of the pulsation periods.

1. INTRODUCTION

The evolved and low-mass Type II Cepheids (hereafter TIIC; for a general review, see Welch 2012) are one of the old population distance indicators. Similar to the young Type I or classical Cepheids, TIIC also exhibit a period-luminosity (PL, or the Leavitt Law) relation. However, TIIC are ~ 2 mag less luminous than the classical Cepheids. Nevertheless, TIIC are a few magnitudes more luminous, depending on the pulsation periods and filters, than the popular RR Lyrae – another old population distance indicator. Therefore, TIIC are useful to probe a more distant stellar system (such as dwarf galaxies and elliptical galaxies) independent of RR Lyrae stars. The comprehensive reviews on TIIC as distance indicators can be found, for examples, in Wallerstein (2002), Sandage & Tammann

(2006), Beaton et al. (2018), Bhardwaj (2020), and Bhardwaj (2022).

Some of the earlier derivations of *BVI*-band, or a subset of these filters, PL relations for TIIC can be found, for examples, in Demers & Wehlau (1971), Nemeč et al. (1994), Alcock et al. (1998), and Pritzl et al. (2003). Other works on the optical PL relations included a color term (Breger & Bregman 1975; Alcock et al. 1998) to derive the period-luminosity-color (PLC) relation, or using the Wesenheit index to derive the equivalent period-Wesenheit (PW) relation (Kubiak & Udalski 2003; Matsunaga et al. 2011; Groenewegen & Jurković 2017). Recently, the optical band PL and PW relations were extended to the filters specific for the *Gaia* mission (Ripepi et al. 2019, 2022). In addition, Groenewegen & Jurković (2017) have also derived the bolometric PL relation based on a combined sample of TIIC in Magellanic Clouds.

Compared to the optical PL relations, more studies have derived TIIC PL and PW relations in the near-

infrared *JHK* bands, or a subset of these filters, in the past two decades. These near-infrared PL/PW relations were derived using THIC located in various stellar systems, including globular clusters (Matsunaga et al. 2006), the Galactic Bulge (Groenewegen et al. 2008; Bhardwaj et al. 2017a; Braga et al. 2018), the Large and/or Small Magellanic Cloud (Matsunaga et al. 2009; Ciechanowska et al. 2010; Matsunaga et al. 2011; Ripepi et al. 2015; Bhardwaj et al. 2017b; Wielgórski et al. 2022), and in nearby Milky Way field (Wielgórski et al. 2022). Some of the derived *K*-band PL relations in the Galactic bulge also included an additional dependence on the Galactic longitude and latitude (Groenewegen et al. 2008; Braga et al. 2018).

To our knowledge, there is no *ugrizY*-band PL and PW relations available in the literature, which will be important in the era of Vera Rubin Observatory Legacy Survey of Space and Time (LSST, Ivezić et al. 2019). Therefore, the goal of this work is to derive the *gri*-band PL and PW relations, by utilizing the time-series observations from the Zwicky Transient Facility (ZTF, Bellm & Kulkarni 2017; Bellm et al. 2019; Dekany et al. 2020; Graham et al. 2019) project and archival data compiled in Bhardwaj (2022), because ZTF cannot observe the southern sky, for THIC located in the globular clusters. THIC in globular clusters have been used to derive PL relations in the past. Demers & Harris (1974) derived the *V*-band PL relation based on 17 THIC found in 4 globular clusters, while Pritzl et al. (2003) derived the *BVI*-band PL relations using two globular clusters (NGC 6388 and NGC 6441) that host the most THIC (for a total of 10 THIC). Optical and near-infrared PL relations were also derived from a larger sample of THIC in Nemec et al. (1994, with ~ 40 THIC in 15 globular clusters) and Matsunaga et al. (2006, with 46 THIC in 26 globular clusters), respectively. Note that PL relations presented in Matsunaga et al. (2006) were updated in Braga et al. (2020) and Bhardwaj (2022).

Section 2 describes the THIC sample and their ZTF light curves data used in this work. In Section 3, we refined the pulsation periods and determined the mean magnitudes for our sample of THIC. The derivations of the PL relations are presented in Section 4, as well as the multi-band relations (PW and period-color relations) in Section 5. We tested our derived PL/PW relations for a sample of M31 THIC in Section 6, followed by conclusions of our work in Section 7.

2. SAMPLE AND DATA

2.1. Selecting THIC in Globular Clusters

We started the compilation of THIC in globular clusters using the “Updated Catalog of Variable Stars in

Globular Clusters” (Clement et al. 2001; Clement 2017, hereafter Clement’s Catalog), by selecting globular clusters that can be observed with ZTF ($\delta_{J2000} > -30^\circ$) and variable stars marked as “CW”, “CWA”, “CWB”, “RV”, or “RVB” in the Clement’s Catalog.¹ The known foreground or suspected foreground THIC in the Clement’s Catalog (marked with an “f” or “f?”), however, were excluded. The preliminary list of THIC were augmented with the catalogs presented in Pritzl et al. (2003) and Matsunaga et al. (2006). We have also searched the literature for new THIC, and updated equatorial coordinates, periods, and classifications of THIC in our preliminary list. We identified five new, or re-classified, THIC: V24 in M10 (Rozyczka et al. 2018), V167 in M14 (Yepez et al. 2022), V34 and ZK3 in M15 (Bhardwaj et al. 2021), and V24 in M22 (Rozyczka et al. 2017). Similarly, we rejected the THIC that were re-classified as other types of variable stars in recent work, they included V1 in M10 (identified as a semi-regular variable in Rozyczka et al. 2018), V72 and V142 in M15 (identified as a RR Lyrae and an anomalous Cepheid, respectively, in Bhardwaj et al. 2021), V21 and V22 in M28 (identified as a long-period variable and a RR Lyrae, respectively, in Prieto et al. 2012), V8 in M79 (identified as a semi-regular variable in Bond et al. 2016), and V7 in M92 (identified as an anomalous Cepheid in Osborn et al. 2012). We also excluded S7 in M3 because the position of this variable star coincides with V254, a known RR Lyrae. All together, our preliminary list contains 50 THIC located in 23 globular clusters.

2.2. Extracting ZTF Light-Curves

ZTF is a wide-field synoptic survey on the northern sky observed in *gri* filters. Combining the Samuel Oschin 48 inch Schmidt telescope (located at the Palomar Observatory) and a dedicated wide-field mosaic CCD camera, the field-of-view of ZTF can reach to 47 squared degrees, while maintaining a pixel scale of 1.01"/pixel. ZTF carries out three high-level surveys: the partner surveys, the public surveys, and the Caltech (California Institute of Technology) surveys. Imaging data from all of these high-level surveys were processed

¹ Classifications of variable stars in the Clement’s Catalog were based on the GCVS (General Catalog of Variable Stars) classification, available at <http://www.sai.msu.su/gcvs/gcvs/vartype.htm>. In brief, “CW” refers to W Virginis type, “CWA” and “CWB” are subtypes of “CW” with pulsation periods separated at 8 days. “RV” refers to the RV Tauri type, and “RVB” is subtype of “RV” which exhibits long-term periodic variations. Both W Virginis and RV Tauri are also subtypes of THIC.

through a dedicated reduction pipeline (Masci et al. 2019), and the photometry were calibrated to the Pan-STARRS1 (Panoramic Survey Telescope and Rapid Response System 1, Chambers et al. 2016; Magnier et al. 2020) AB magnitude system. The preliminary list of THIC sample were cross-matched to the PSF (point-spread function) catalogs, generated from the reduction pipeline, using an $1''$ search radius. The extracted *gri*-band (whenever available) light-curves for these THIC were based on the ZTF Public Data Release 10 (DR10) data and partner surveys data until 2022 March 31. Out of the preliminary 50 THIC sample, 48 of them have ZTF light-curves in at least two of the *gri* filters (there are 1 and 11 THIC without the *g*- and *i*-band light curves, respectively). The number of data points per light curve varies from 1 to ~ 1500 for the extracted light curves, with medians of 158, 504, and 51 in the *gri*-band, respectively. Two THIC without ZTF light-curves are V1 and V2 in M19.

3. PERIODS AND MEAN MAGNITUDES

Since it is well-known that THIC will undergo periods change (for examples, see Wehlau & Bohlender 1982; Percy et al. 1997; Percy & Hoss 2000; Schmidt et al. 2004, 2005a,b; Rabidoux et al. 2010; Osborn et al. 2012; Soszyński et al. 2018; Karmakar et al. 2019; Berdnikov & Pastukhova 2021, roughly in the range of $\sim 10^{-8}$ to $\sim 10^{-11}$ days/day), we re-determined the periods of our sample of THIC with ZTF light curves instead of adopting the published periods.

Given that majority of our sample of THIC have ZTF light curves in two or three filters, we employed the `LombScargleMultiband` module available in the `astroML/gatspy`² package (VanderPlas & Ivezić 2015) to refine the periods for our sample of THIC in a two-steps process. In the first step, ZTF light-curves were folded using periods identified from the first-pass of `LombScargleMultiband`, and then fit with a low-order Fourier expansion in the following form (for example, see Deb & Singh 2009):

$$m(\Phi) = m_0 + \sum_{j=1}^n [a_j \cos(2\pi j\Phi) + b_j \sin(2\pi j\Phi)], \quad (1)$$

where $\Phi \in [0, 1]$ are the pulsational phases. Note that we only fit equation (1) to the light curves that have more than 30 data points. Outliers beyond 3σ were excluded, where σ represents the dispersion of the fitted light

curves, and `LombScargleMultiband` was run again in the second-pass to obtain the final adopted periods. The periods obtained from `LombScargleMultiband` need to be doubled for three THIC (V11 in M2, V84 in M5, and V6 in M56) in order to match with published periods. We found that the period for V6 in M2 also needs to be doubled, because alternate minima can be seen on its light-curves (as displayed in Figure 1).

We visually inspected all light-curves folded with the final adopted periods. We removed 9 THIC (V1 in M12, V12 in M13, V34 in M15, V17 and V32 in M28, V22 in NGC6229, V2 in NGC6293, V4 in NGC7492, and V4 in Pal3) from our sample because they exhibit evidence of blending (such as no variations or large scatters seen on the ZTF light-curves). We further removed 2 THIC (V154 in M3 and V3 in M10) that only have 19 data points in the *r*-band light-curve (and the total number of data points in all three filters is 30 or less). Finally, 37 THIC remained in our sample and their intensity mean magnitudes were obtained based on the fitted low-order Fourier expansion as given in equation (1). The final adopted periods and the intensity mean magnitudes of these THIC are listed in Table 1. Examples of the ZTF light-curves are presented in Figure 2.

4. THE PL RELATIONS

4.1. Preliminary PL Relations

Homogeneous and accurate distances of globular clusters were adopted from Baumgardt & Vasiliev (2021), who combined various distance measurements based on the *Gaia* and/or *Hubble Space Telescope* data, as well as literature distances, to obtain averaged distances via a likelihood analysis. Using these distances, we queried the `Bayerstar2019` 3D reddening map (Green et al. 2019)³ via the `dustmaps`⁴ (Green 2018) code to obtain reddening E towards each of the THIC, and corrected the extinctions on mean magnitudes using $A_g = 3.518E$, $A_r = 2.617E$ and $A_i = 1.971E$ (Green et al. 2019). A linear regression was fitted to the extinction-corrected absolute magnitudes for 37 and 17 THIC in the *gr*- and *i*-band, respectively. While fitting the PL relations, we did not separate the THIC into the three sub-types (BL Hercules, W Virginis, and RV Tauri) of THIC, mainly due to the small number of samples in each subtype.

We compare our preliminary *gri*-band PL relations to the Johnson-Cousin *BVI*-band and 2MASS *JHK*-band (hereafter collectively referred as *BVIJHK*-band) PL relations, taken from Bhardwaj (2022), in the left

² <https://github.com/astroML/gatspy>, also see VanderPlas (2016).

³ See <http://argonaut.skymaps.info/usage>

⁴ <https://dustmaps.readthedocs.io/en/latest/>

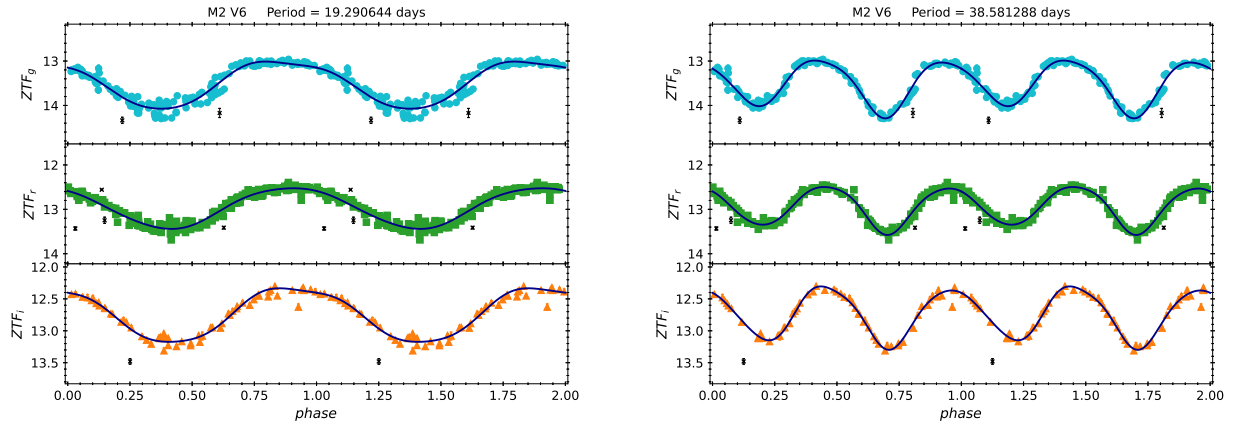


Figure 1. ZTF light-curves for V6 in M2 folded with the period determined from `LombScargleMultiband` (left panel) and twice of the determined period (right panel). Alternate minima can be seen when the determined period is doubled. The black curves are fitted low-order Fourier expansion given in equation (1). Crosses are rejected outliers based on the two-steps fitting process (see text for details).

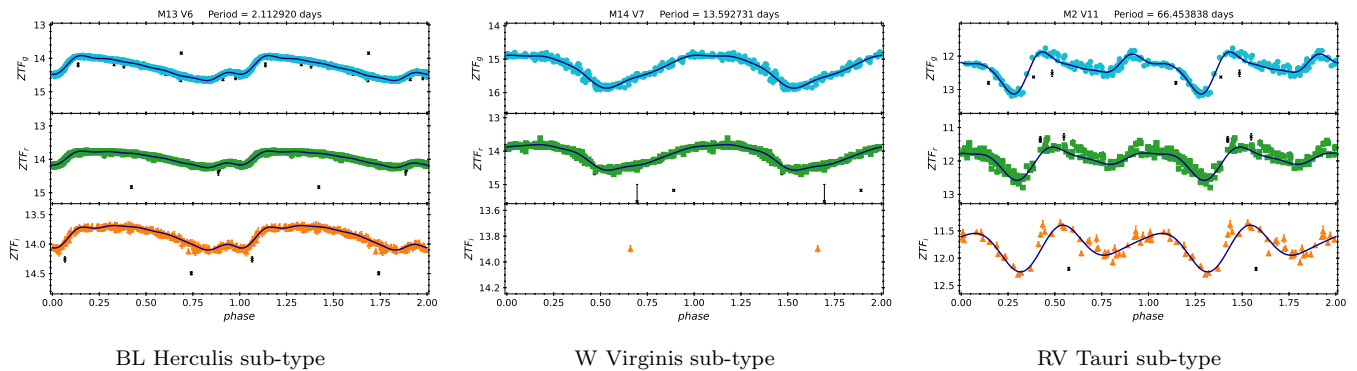


Figure 2. Examples of ZTF light curves for TIIC in three different period ranges, roughly represent the three sub-types (BL Herculis, W Virginis, and RV Tauri) of TIIC. The black curves are fitted low-order Fourier expansion given in equation (1). Crosses are rejected outliers based on the two-steps fitting process (see text for details).

panel of Figure 3. The slopes of the *gri*-band PL relations follow the trend that the slopes become steeper at longer wavelengths, however these *gri*-band PL slopes were shallower than the expected trends portrait from the *BVIJHK*-band PL slopes. Similar to our work, the *BVIJHK*-band PL relations were derived by Bhardwaj (2022) using a sample of 36 to 50 TIIC in globular clusters compiled from the literature. The distance moduli of these globular clusters were collected in Braga et al. (2020). In contrast to our work, these distance moduli were compiled from various publications (see the reference listed in Table 4 of Braga et al. 2020). In the next sub-section, we demonstrate that after updating the multi-band PL relations, the *gri*-band PL slopes are consistent with the *BVI*-band PL slopes, as shown in the upper-right panel of Figure 3. Similarly, the dispersion of the preliminary *gri*-band PL relations were larger

(especially in the *i*-band), and improvements were evident after updating the PL relations.

4.2. Updated the PL Relations

We updated the *BVIJHK*-band PL relations for the TIIC sample compiled in Bhardwaj (2022, hereafter B22 sample) by adopting the homogeneous distance from Baumgardt & Vasiliev (2021) to their host globular clusters. We have also adopted the homogeneous reddening $E(B - V)$ queried from the same all-sky “SFD” dust map (Schlegel et al. 1998), using the `dustmaps` code, to the TIIC in B22 sample. The compiled *BVIJHK*-band mean magnitudes (whenever available), as well as the adopted distances and reddenings, for the B22 sample are presented in Table 2. Mean magnitudes in the *BVI*-band were adopted from various sources as listed in the last column of Table 2. For *JHK*-band mean magnitudes, majority of them were taken from Matsunaga et al. (2006) except for V34 in M15

Table 1. Basic Information and Mean Magnitudes for ZTF Sample of THIC in Globular Clusters

G. C.	Var. Name	P_{lit}^a (days)	P (days)	N_g	N_r	N_i	$\langle g \rangle$	$\langle r \rangle$	$\langle i \rangle$	D^b (kpc)	E^c	Note ^d
M15	V1	1.43781	1.437812	540	665	135	15.029	14.837	14.754	10.71 ± 0.10	0.068 ± 0.002	1
M13	V1	1.45902	1.459040	1067	1103	215	14.173	14.037	14.011	7.42 ± 0.08	0.000 ± 0.000	3
M56	V1	1.51000	1.509997	392	851	31	15.685	15.232	15.049	10.43 ± 0.14	0.202 ± 0.002	8
NGC2419	V18	1.57870	1.578572	379	1078	63	19.032	18.733	18.633	88.47 ± 2.40	0.144 ± 0.004	8
M22	V11	1.69050	1.690401	77	581	0	12.835	12.230	...	3.30 ± 0.04	0.419 ± 0.006	8
M22	V24	1.71485	1.715079	76	581	0	13.746	13.130	...	3.30 ± 0.04	0.419 ± 0.006	5
M15	ZK3	1.74634	1.746591	537	667	134	15.361	15.000	14.799	10.71 ± 0.10	0.162 ± 0.004	1
NGC6401	V3	1.74870	1.747028	83	343	71	17.092	15.947	15.317	8.06 ± 0.24	0.926 ± 0.002	8
M14	V76	1.88990	1.890065	182	569	1	16.329	15.508	...	9.14 ± 0.25	0.540 ± 0.000	7
M13	V6	2.11286	2.112920	1049	1077	215	14.271	13.962	13.854	7.42 ± 0.08	0.000 ± 0.000	3
M10	V24	2.30746	2.307591	71	142	1	14.355	13.728	...	5.07 ± 0.06	0.312 ± 0.002	6
M19	V4	2.43260	2.432354	62	411	0	15.555	14.943	...	8.34 ± 0.16	0.488 ± 0.005	8
M14	V2	2.79490	2.794852	182	582	1	15.955	15.093	...	9.14 ± 0.25	0.540 ± 0.000	7
NGC6284	V4	2.81870	2.818707	63	486	0	16.029	15.446	...	14.21 ± 0.42	0.318 ± 0.002	8
NGC6749	V1	4.48100	4.477411	125	296	2	18.515	16.633	...	7.59 ± 0.21	1.346 ± 0.007	8
NGC6284	V1	4.48120	4.484024	66	493	0	15.806	15.131	...	14.21 ± 0.42	0.318 ± 0.002	8
M13	V2	5.11078	5.111326	1071	1097	216	13.157	12.882	12.787	7.42 ± 0.08	0.000 ± 0.000	3
M14	V167	6.20100	6.205786	182	564	1	16.046	14.965	...	9.14 ± 0.25	0.560 ± 0.003	7
NGC6325	V2	10.74400	10.748907	66	498	0	16.533	14.938	...	7.53 ± 0.32	0.966 ± 0.005	8
M14	V17	12.07580	12.092216	184	582	1	15.189	14.123	...	9.14 ± 0.25	0.540 ± 0.000	7
NGC6325	V1	12.51600	12.522716	65	497	0	16.299	14.716	...	7.53 ± 0.32	0.928 ± 0.006	8
M28	V4	13.46200	13.480377	136	909	144	13.532	12.558	12.093	5.37 ± 0.10	0.458 ± 0.004	8
M14	V7	13.58970	13.592731	185	581	1	15.222	14.104	...	9.14 ± 0.25	0.560 ± 0.003	7
M79	V7	13.99950	14.057529	114	136	0	13.824	13.304	...	13.08 ± 0.18	0.014 ± 0.002	2
NGC6229	V8	14.84600	14.844260	1469	1484	431	15.699	15.117	14.939	30.11 ± 0.47	0.092 ± 0.002	8
M2	V1	15.56470	15.542598	61	70	6	13.596	13.075	...	11.69 ± 0.11	0.000 ± 0.000	8
M80	V1	16.28134	16.306309	62	74	0	13.734	13.097	...	10.34 ± 0.12	0.220 ± 0.003	4
M19	V3	16.50000	16.686135	66	421	0	14.128	13.157	...	8.34 ± 0.16	0.488 ± 0.005	8
M15	V86	16.84211	16.833319	514	650	133	13.112	12.553	12.353	10.71 ± 0.10	0.162 ± 0.004	1
M2	V5	17.55700	17.574309	132	215	53	13.572	13.015	12.831	11.69 ± 0.11	0.004 ± 0.004	8
M10	V2	19.47099	18.713201	146	333	2	12.211	11.504	...	5.07 ± 0.06	0.312 ± 0.002	6
M14	V1	19.74110	18.749399	184	581	1	14.762	13.692	...	9.14 ± 0.25	0.568 ± 0.002	7
M5	V42	25.73500	25.710120	199	316	75	11.457	11.123	10.927	7.48 ± 0.06	0.090 ± 0.000	8
M2	V6	19.29900	38.581288	156	257	61	13.438	12.892	12.696	11.69 ± 0.11	0.000 ± 0.000	8
M5	V84	53.95000	52.934619	245	424	100	11.626	11.231	11.039	7.48 ± 0.06	0.112 ± 0.002	8
M2	V11	67.00000	66.453838	132	218	50	12.300	11.933	11.755	11.69 ± 0.11	0.000 ± 0.000	8
M56	V6	90.00000	89.320054	391	857	31	13.278	12.386	11.827	10.43 ± 0.14	0.202 ± 0.002	8

^a Period published in the literature.

^b Distance of the globular clusters adopted from [Baumgardt & Vasiliev \(2021\)](#).

^c Reddening returned from the Bayerstar2019 3D reddening map ([Green et al. 2019](#)) at the location of the THIC with distance D from [Baumgardt & Vasiliev \(2021\)](#).

^d Literature period adopted from the following reference: 1 = [Bhardwaj et al. \(2021\)](#); 2 = [Bond et al. \(2016\)](#); 3 = [Osborn et al. \(2019\)](#); 4 = [Plachy et al. \(2017\)](#); 5 = [Rozycka et al. \(2017\)](#); 6 = [Rozycka et al. \(2018\)](#); 7 = [Yepez et al. \(2022\)](#); 8 = Clement's Catalog.

([Bhardwaj et al. 2021](#)) and V43, V60, V61, and V92 in NGC 5139 ([Braga et al. 2020](#)). We excluded V1 in M10 and V8 in M79 from the B22 sample for the reasons mentioned in Section 2.1.

The JHK photometry from the aforementioned three studies was homogeneously calibrated to 2MASS (2 Micron All Sky Survey, [Skrutskie et al. 2006](#)) system. However, the optical photometric data are very heterogeneous and were taken from several different studies as evident from the last column of Table 2. Since most of

the mean magnitudes do not have their associated photometric measurement errors and are likely to suffer from systematic uncertainties, we adopt an error of 0.05 magnitudes on the mean magnitudes. The available mean magnitudes listed in Table 2 were converted to absolute magnitudes using the adopted distances. Extinction corrections on $BVIJHK$ -band mean magnitudes were done using $A_{BVIJHK} = R_{BVIJHK}E(B - V)$, where $R_{BVIJHK} = \{3.626, 2.742, 1.505, 0.793, 0.469, 0.303\}$ ([Schlafly & Finkbeiner 2011](#); [Green et al. 2019](#)). We

Table 2. Basic Information and Mean Magnitudes for B22 Sample of THC in Globular Clusters

G. C.	Var. Name	P (days)	B	V	I	J	H	K	D^a (kpc)	$E(B - V)^b$	Reference ^c
NGC5139	V43	1.1569	14.139	13.759	13.149	12.730	12.492	12.426	5.43 ± 0.05	0.14	3
NGC5139	V92	1.346	14.480	13.946	13.199	12.700	12.340	12.313	5.43 ± 0.05	0.13	3
NGC5139	V60	1.3495	14.028	13.624	13.001	12.584	12.295	12.281	5.43 ± 0.05	0.14	3
M15	V1	1.4377	15.412	14.954	14.362	13.94	...	13.65	10.71 ± 0.10	0.11	8
M56	V1	1.51	16.01	15.46	...	13.99	13.66	13.57	10.43 ± 0.14	0.25	18
M62	V73	1.7	16.147	15.243	13.966	6.41 ± 0.10	0.45	6, 17
NGC2808	V10	1.7653	15.91	15.28	14.47	13.89	13.54	13.43	10.06 ± 0.11	0.22	12
M14	V76	1.8903	16.881	15.978	14.750	13.78	13.30	13.16	9.14 ± 0.25	0.48	7
M15	V34	2.03355	13.756	...	13.340	10.71 ± 0.10	0.11	
NGC5139	V61	2.2736	14.293	13.661	12.821	12.190	11.811	11.771	5.43 ± 0.05	0.14	3
M19	V4	2.4326	14.75	...	13.947	13.28	12.85	12.77	8.34 ± 0.16	0.31	4, 17
NGC6441	V132	2.5474	17.218	16.478	15.241	12.73 ± 0.16	0.61	13
M14	V2	2.7947	16.596	15.629	14.337	13.45	12.98	12.85	9.14 ± 0.25	0.48	7
NGC6284	V4	2.8187	16.04	...	14.786	14.15	13.71	13.67	14.21 ± 0.42	0.31	5, 17
NGC5139	V48	4.4752	13.528	12.924	12.092	11.59	11.14	11.15	5.43 ± 0.05	0.14	3
NGC6749	V1	4.481	13.38	12.62	12.34	7.59 ± 0.21	1.75	
NGC6284	V1	4.4812	15.88	...	14.504	13.68	13.24	13.18	14.21 ± 0.42	0.30	5, 17
M10	V3	7.831	13.62	12.75	11.721	11.02	10.55	10.36	5.07 ± 0.06	0.27	2, 15
NGC6441	V153	9.89	13.72	12.73 ± 0.16	0.62	16
M62	V2	10.59	14.408	13.418	12.065	11.22	10.64	10.53	6.41 ± 0.10	0.47	6, 17
NGC6325	V2	10.744	13.632	12.14	11.43	11.22	7.53 ± 0.32	0.96	17
NGC6441	V154	10.83	13.57	12.73 ± 0.16	0.61	16
M14	V17	12.091	15.846	14.676	13.182	9.14 ± 0.25	0.47	7
NGC6256	V1	12.447	13.402	11.86	11.15	10.85	7.24 ± 0.29	1.71	17
NGC6325	V1	12.516	13.436	11.97	11.25	11.02	7.53 ± 0.32	0.95	17
M28	V4	13.462	14.21	...	11.734	10.78	10.18	10.01	5.37 ± 0.10	0.49	17, 19
NGC6441	V128	13.519	16.475	15.257	13.795	12.73 ± 0.16	0.61	13
M14	V7	13.6038	16.051	14.745	13.224	12.04	11.46	11.29	9.14 ± 0.25	0.48	7
M19	V2	14.139	14.15	...	12.242	11.53	11.06	10.92	8.34 ± 0.16	0.32	4, 17
HP1	V17	14.42	11.91	11.09	10.78	7.00 ± 0.14	2.32	
NGC5139	V29	14.7338	12.776	12.015	11.049	10.43	10.03	9.93	5.43 ± 0.05	0.14	3
M3	V154	15.29	12.79	12.33	11.68	11.45	11.06	10.99	10.18 ± 0.08	0.01	14
M12	V1	15.527	10.24	9.79	9.64	5.11 ± 0.05	0.18	
M2	V1	15.5647	13.97	13.36	...	11.93	11.54	11.45	11.69 ± 0.11	0.04	9
M80	V1	16.3042	14.19	13.365	...	11.65	11.23	11.10	10.34 ± 0.12	0.21	11, 20
HP1	V16	16.4	11.77	10.99	10.70	7.00 ± 0.14	2.39	
M19	V3	16.5	13.70	...	12.417	8.34 ± 0.16	0.31	4, 17
M15	V86	16.829	14.368	13.659	12.646	11.70	11.32	11.19	10.71 ± 0.10	0.11	8
M19	V1	16.92	13.85	...	12.260	11.37	10.88	10.75	8.34 ± 0.16	0.32	4, 17
M2	V5	17.557	13.89	13.28	...	11.80	11.40	11.31	11.69 ± 0.11	0.04	9
NGC6441	V129	17.832	16.395	15.128	13.610	12.14	11.61	11.65	12.73 ± 0.16	0.62	13
M10	V2	18.7226	13.01	12.05	10.934	10.05	9.61	9.47	5.07 ± 0.06	0.29	2, 15
M14	V1	18.729	15.429	14.210	12.633	11.63	11.10	10.89	9.14 ± 0.25	0.48	7
Terzan1	V5	18.85	14.576	11.97	10.93	10.61	5.67 ± 0.17	6.86	17
M2	V6	19.299	13.74	13.14	...	11.72	11.33	11.25	11.69 ± 0.11	0.04	9
NGC6441	V127	19.773	16.398	15.048	13.441	12.73 ± 0.16	0.61	13
NGC6441	V126	20.625	16.282	14.997	13.402	12.73 ± 0.16	0.61	13
NGC6441	V6	21.365	16.117	14.885	13.231	12.16	11.64	11.49	12.73 ± 0.16	0.61	13
M5	V42	25.735	11.82	11.659	10.740	10.16	9.85	9.82	7.48 ± 0.06	0.04	1, 14
M5	V84	26.87	12.11	11.287	10.451	10.20	9.80	9.71	7.48 ± 0.06	0.04	1, 14
NGC6453	V2	27.1954	...	14.231	12.375	11.35	10.75	10.59	10.07 ± 0.22	0.66	17
NGC5139	V1	29.3479	11.488	10.829	10.058	9.40	9.05	8.99	5.43 ± 0.05	0.13	3
NGC6453	V1	31.0476	...	14.601	12.789	11.51	10.85	10.66	10.07 ± 0.22	0.66	17
M2	V11	33.4	12.67	12.11	...	10.87	10.53	10.44	11.69 ± 0.11	0.04	9
NGC5986	V13	40.62	10.90	10.22	10.07	10.54 ± 0.13	0.34	
M56	V6	45.0	13.7	12.9	...	10.86	10.37	10.21	10.43 ± 0.14	0.25	18
M28	V17	48.0	9.55	8.95	8.75	5.37 ± 0.10	0.49	
NGC6569	V16	87.5	16.55	10.56	9.74	9.45	10.53 ± 0.26	0.43	10

^aDistance of the globular clusters adopted from [Baumgardt & Vasiliev \(2021\)](#).^bReddening returned from the ‘‘SFD’’ dust map ([Schlegel et al. 1998](#)).^cSources for the BVI -band mean magnitudes: 1 = [Arellano Ferro et al. \(2016\)](#); 2 = [Arellano Ferro et al. \(2020\)](#); 3 = [Braga et al. \(2020\)](#); 4 = [Clement & Hogg \(1978\)](#); 5 = [Clement et al. \(1980\)](#); 6 = [Contreras et al. \(2010\)](#); 7 = [Contreras Peña et al. \(2018\)](#); 8 = [Corwin et al. \(2008\)](#); 9 = [Demers \(1969\)](#); 10 = [Hazen-Liller \(1985\)](#); 11 = [Kopacki \(2013\)](#); 12 = [Kunder et al. \(2013\)](#); 13 = [Pritzl et al. \(2003\)](#); 14 = [Rabidoux et al. \(2010\)](#); 15 = [Rozyczka et al. \(2018\)](#); 16 = [Skottfelt et al. \(2015\)](#); 17 = [Udalski et al. \(2018\)](#); 18 = [Wehlau & Hogg \(1985\)](#); 19 = [Wehlau & Butterworth \(1990\)](#); 20 = [Wehlau et al. \(1990\)](#).

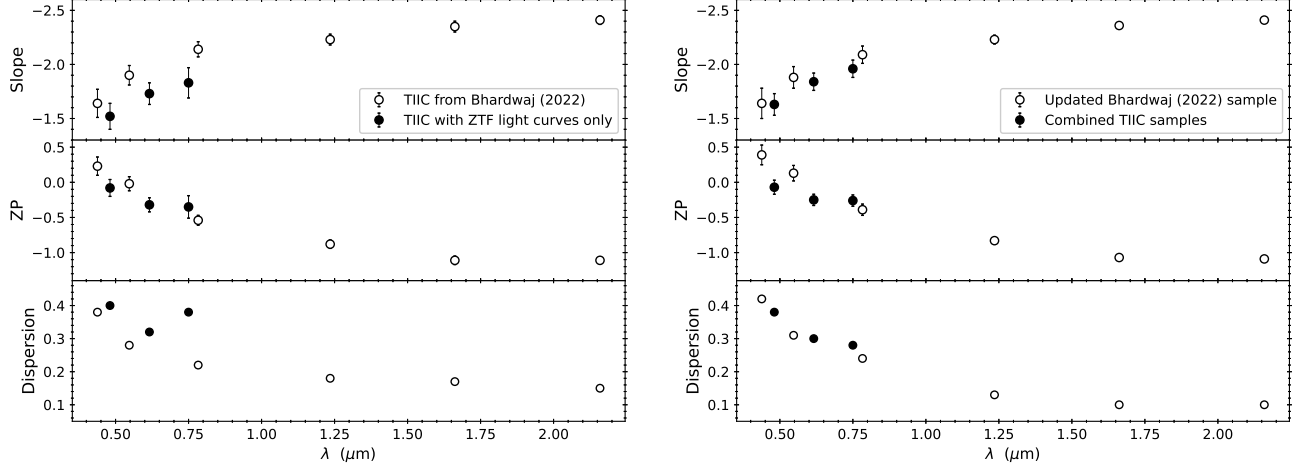


Figure 3. **Left Panel:** Comparison of the slopes (upper panel), zero-points (ZP, middle panel), and the dispersions (lower panel) for PL relations derived in Bhardwaj (2022, for *BVIJHK*-band, in open symbols) and the preliminary *gri*-band PL relations using TIIC listed in Table 1 (in filled symbols). **Right Panel:** Same as the left panel, but for the updated PL relations as described in Section 4.2.

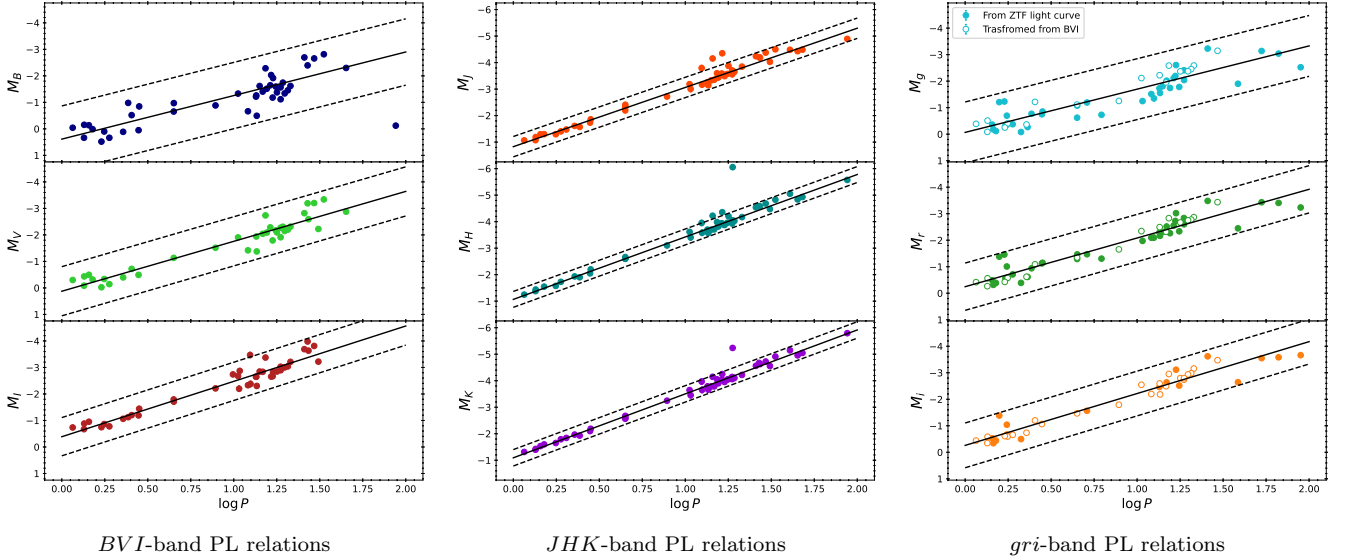


Figure 4. The updated multi-band PL relations, where the best-fit PL relations are shown in solid lines (see Table 3), and the dashed lines represent the $\pm 3\sigma$ of the best-fit PL relations (hence, data points outside the $\pm 3\sigma$ range are rejected in the fitting). The *BVIJHK*-band PL relations were updated from Bhardwaj (2022) by using the homogeneous distance from Baumgardt & Vasiliev (2021). The updated *gri*-band PL relations were derived from combining two samples of TIIC: those with ZTF data as listed in Table 1, and the TIIC from B22 sample that are not included in Table 1 (after transformed to the *gri* bands). See Section 4.2 for more details. Note that the error bars are smaller than the size of the symbols.

Table 3. The Derived Period-Luminosity Relations for THIC in the Globular Clusters

Band	a	b	σ	N
<i>B</i>	-1.64 ± 0.14	0.39 ± 0.14	0.42	42
<i>V</i>	-1.88 ± 0.10	0.13 ± 0.11	0.31	37
<i>I</i>	-2.09 ± 0.08	-0.39 ± 0.08	0.24	41
<i>J</i>	-2.23 ± 0.04	-0.83 ± 0.04	0.13	45
<i>H</i>	-2.36 ± 0.03	-1.07 ± 0.04	0.10	43
<i>K</i>	-2.41 ± 0.03	-1.09 ± 0.03	0.10	48
<i>g</i>	-1.63 ± 0.10	-0.07 ± 0.10	0.38	55
<i>r</i>	-1.84 ± 0.08	-0.25 ± 0.08	0.30	55
<i>i</i>	-1.96 ± 0.08	-0.26 ± 0.08	0.28	41

NOTE—The PL relation takes the form of $m = a \log P + b$, and σ is the dispersion of the fitted PL relation. N represents the number of THIC used in the fitting.

then fit the PL relations using an iterative 3σ -clipping linear regression (where σ is the dispersion of the regression), implemented in `astropy`, to exclude a few obvious outliers. The updated *BVIJHK*-band PL relations are shown in Figure 4 and provided in Table 3.

There are 33 THIC in the B22 sample that are not included in Table 1. Majority of these THIC were located at south of $\delta_{J2000} = -30^\circ$ (i.e. outside the ZTF footprint), and the remaining THIC either did not have ZTF light curve data or were excluded (e.g. due to blending). The *BVI*-band mean magnitudes for these THIC, whenever available, were transformed to the *gri*-band using the transformations provided in Tonry et al. (2012). Extinction corrections were done using the `Bayerstar2019` 3D reddening map if available, else the “SFD” dust map was used together with the conversion of $E = E(B - V)/0.884$ (see footnote 3). Similarly, there are 25 common THIC in B22 sample and Table 1,⁵ the *BVI*-band mean magnitudes from B22 sample were transformed to the *i*-band for those THIC without the *i*-band data. Open circles in the right panels of Figure 4 represent the THIC in B22 sample transformed from the *BVI*-band photometry.

⁵ We checked the consistency of transformed *gri*-band mean magnitudes using the 25 common THIC in B22 sample and Table 1. The averaged differences of $m_{ZTF} - m_T$ in the *gri*-band are 0.014, -0.123 , and -0.020 mag, respectively, where m_{ZTF} and m_T represent the ZTF and the transformed mean magnitudes. The corresponding standard deviations in the *gri*-band are 0.092, 0.163, and 0.160 mag, respectively. Note that after removing an extreme outlier, the number of THIC in both samples with mean magnitudes to calculate the averaged difference is 16 for the *gr*-band, and 3 for the *i*-band. The revised *r*-band PL relation, $M_r = -1.83(\pm 0.08) \log P - 0.29(\pm 0.08)$ with $\sigma = 0.31$ mag, is consistent with Table 3 after taking the averaged differences of -0.12 mag into account.

Combining the THIC in Table 1 and those transformed from B22 sample, we derived the updated *gri*-band PL relation, using the same iterative 3σ -clipping linear regression. The results are listed in the bottom part of Table 3. With the updated PL relations, derived using the homogeneous distances, consistent PL relations were found between the *BVI*-band PL relations and the *gri*-band PL relations, as demonstrated in the right-panel of Figure 3.

Most of the previous studies have suggested that the PL relations for THIC are insensitive to metallicity (for examples, see Matsunaga et al. 2006; Di Criscienzo et al. 2007; Matsunaga et al. 2009; Ciechanowska et al. 2010; Ripepi et al. 2015; Groenewegen & Jurkovic 2017; Braga et al. 2018; Bhardwaj 2020, 2022, and reference therein). In contrast, significant metallicity terms were found for the *UB*-band and *JHK*-band PL relations from theoretical work of Das et al. (2021) and empirical investigations of Wielgórski et al. (2022), respectively. Following Matsunaga et al. (2006) and Wielgórski et al. (2022), we fit a linear regression to the residuals of PL relations as a function of metallicity for our sample of THIC, where the metallicities, $[\text{Fe}/\text{H}]$ for the host globular clusters, were taken from the GOTHAM (GlObular clusTer Homogeneous Abundances Measurements) survey⁶ (Dias et al. 2015, 2016a,b; Vázquez et al. 2018). Metallicity of these host globular clusters ranged from -2.27 dex (M15) to -0.47 dex (NGC6441). Slopes of these linear regressions, denoted as γ , as a function of filters are displayed in Figure 5. Except in *B*-band, the values of γ are consistent with zero in all other filters, implying the corresponding PL relations are insensitive to metallicity. This is consistent with the theoretical predictions of Das et al. (2021). For *B*-band, fitting a period-luminosity-metallicity relation to the data yields:

$$M_B = 0.68(\pm 0.25) - 1.67(\pm 0.14) \log P + 0.19(\pm 0.14)[\text{Fe}/\text{H}], \quad \sigma = 0.41.$$

5. THE MULTI-BAND RELATIONS

In addition to PL relations, the updated B22 samples can be used to derive the period-Wesenheit (PW), period-color (PC), and the period-*Q*-index (PQ) relations in the *BVIJHK*-band. The Wesenheit index, W , is analog to magnitude but it is extinction-free by construction (Madore 1982; Madore & Freedman 1991). Similarly, the *Q*-index is analog to color but

⁶ http://www.sc.eso.org/~bdias/files/dias+16_MWGC.txt

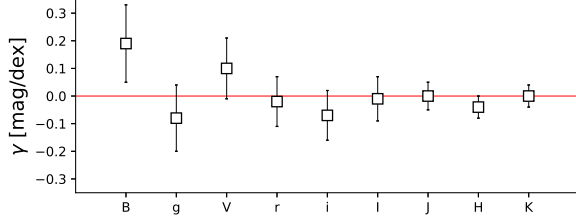


Figure 5. Slopes of the fitted linear regressions, γ , to the plots for PL residuals vs. $[\text{Fe}/\text{H}]$ as a function of filters. The red line indicates the case of $\gamma = 0$.

Table 4. The Derived Period-Wesenheit Relations for TIIC in the Globular Clusters

Wesenheit Index	a	b	σ	N
$W_V^{BV} = V - 3.102(B - V)$	-2.62 ± 0.05	-1.00 ± 0.05	0.13	30
$W_V^{VI} = V - 2.217(V - I)$	-2.43 ± 0.07	-0.99 ± 0.08	0.20	30
$W_B^{BI} = B - 1.710(B - I)$	-2.42 ± 0.05	-0.98 ± 0.05	0.14	31
$W_J^{JH} = J - 2.448(J - H)$	-2.49 ± 0.03	-1.44 ± 0.04	0.11	46
$W_K^{HK} = K - 1.825(H - K)$	-2.51 ± 0.03	-1.10 ± 0.04	0.11	45
$W_K^{JK} = K - 0.618(J - K)$	-2.46 ± 0.03	-1.28 ± 0.03	0.08	46
$W_r^{ri} = r - 4.051(r - i)$	-2.26 ± 0.10	-0.34 ± 0.10	0.34	41
$W_r^{gr} = r - 2.905(g - r)$	-2.43 ± 0.11	-0.77 ± 0.11	0.42	55
$W_g^{gi} = g - 2.274(g - i)$	-2.33 ± 0.07	-0.48 ± 0.07	0.26	41

NOTE—The PW relation takes the form of $W = a \log P + b$, and σ is the dispersion of the fitted relation. N represents the number of TIIC used in the fitting.

Table 5. The Derived Period-Color and Period-Q-index Relations for TIIC in the Globular Clusters

Color	a	b	σ	N
$(B - V)$	0.24 ± 0.04	0.35 ± 0.04	0.11	34
$(V - I)$	0.26 ± 0.04	0.50 ± 0.04	0.11	30
$(B - I)$	0.50 ± 0.11	0.75 ± 0.11	0.31	35
$(J - H)$	0.08 ± 0.02	0.27 ± 0.02	0.05	41
$(H - K)$	0.05 ± 0.01	0.02 ± 0.01	0.04	42
$(J - K)$	0.14 ± 0.02	0.29 ± 0.02	0.06	42
$(g - r)$	0.21 ± 0.04	0.18 ± 0.04	0.15	55
$(r - i)$	0.09 ± 0.02	0.04 ± 0.02	0.06	39
$(g - i)$	0.29 ± 0.04	0.17 ± 0.04	0.15	41
Q_{BVI}	0.12 ± 0.03	-0.04 ± 0.03	0.07	27
Q_{JHK}	0.02 ± 0.02	0.21 ± 0.03	0.08	45
Q_{gri}	0.06 ± 0.05	0.11 ± 0.05	0.17	41

NOTE—The PC and PQ relations take the form of $c = a \log P + b$ (where c is for colors or Q -index), and σ is the dispersion of the fitted relation. N represents the number of TIIC used in the fitting.

reddening-free by construction, inspired from the classical work of [Johnson & Morgan \(1953\)](#), who defined the Q -index in UBV -band). The combined sample of TIIC listed in [Table 1](#) and those photometrically transformed from the B22 sample can also be used to derive the gri -band PW, PC, and PQ relations. The gri -band Wesenheit indices were defined in [Ngeow et al. \(2021\)](#), while the various $BVIJHK$ -band Wesenheit indices are defined in [Table 4](#). For the PQ relations, we have $Q_{BVI} = (B - V) - 0.715(V - I)$ and $Q_{JHK} = (J - H) - 1.952(H - K)$ in the $BVIJHK$ -band, while the gri -band Q -index was adopted from [Ngeow et al. \(2022\)](#) as $Q_{gri} = (g - r) - 1.395(r - i)$. The fitted PW and PC/PQ relations are summarized in [Table 4](#) and [5](#), respectively, as well as presented in [Figure 6](#) and [7](#).

The $(H - K)$ and $(r - i)$ PC relations have relatively flat PC slopes with zero-points almost consistent with zero. These explain why the pairs of HK -band and ri -band PL relations are quite similar, especially their PL zero-points are identical within the uncertainties (see [Table 3](#)). We also see that the redder colors, in JHK -band and in $(r - i)$ color, tend to have the smaller PC dispersion. In contrast, the $(B - I)$ PC relation displays the largest dispersion among all the PC relations. In case of the PQ relations, slopes for both of the Q_{JHK} and Q_{gri} PQ relations are statistically consistent with zero, in contrast to the RR Lyrae ([Ngeow et al. 2022](#)). The Q_{BVI} PQ relation is also much shallower than the BVI -band PC relations, and has the smallest dispersion among the three PQ relations.

6. COMPARISON WITH M31 TIIC

The Pan-STARRS1 survey of Andromeda, known as the PAndromeda project, reported a finding of 278 TIIC in the (halo of) M31 galaxy ([Kodric et al. 2018](#)). This sample of M31 TIIC can be used to test the applicability of our derived PL/PW relations. Numerous distance measurements to M31, via various techniques and distance indicators, can be found in the literature. [de Grijs & Bono \(2014\)](#) summarized the distance estimates prior to 2013 and recommended a distance modulus of $\mu = 24.46 \pm 0.10$ mag to M31. A latest distance measurement to M31 can be found in [Li et al. \(2021\)](#), who give $\mu = 24.407 \pm 0.032$ mag based on the Hubble Space Telescope observations of classical Cepheids.

[Kodric et al. \(2018\)](#) provided the pulsation periods as well as the extinction-corrected gri -band mean magnitudes for these sample of M31 TIIC. We first removed six TIIC that have errors on the periods which are larger than 1 day (or fractional error larger than 1%; the rest of the TIIC have fractional errors that are less than 0.64% in period). The reddening-corrected colors for the re-

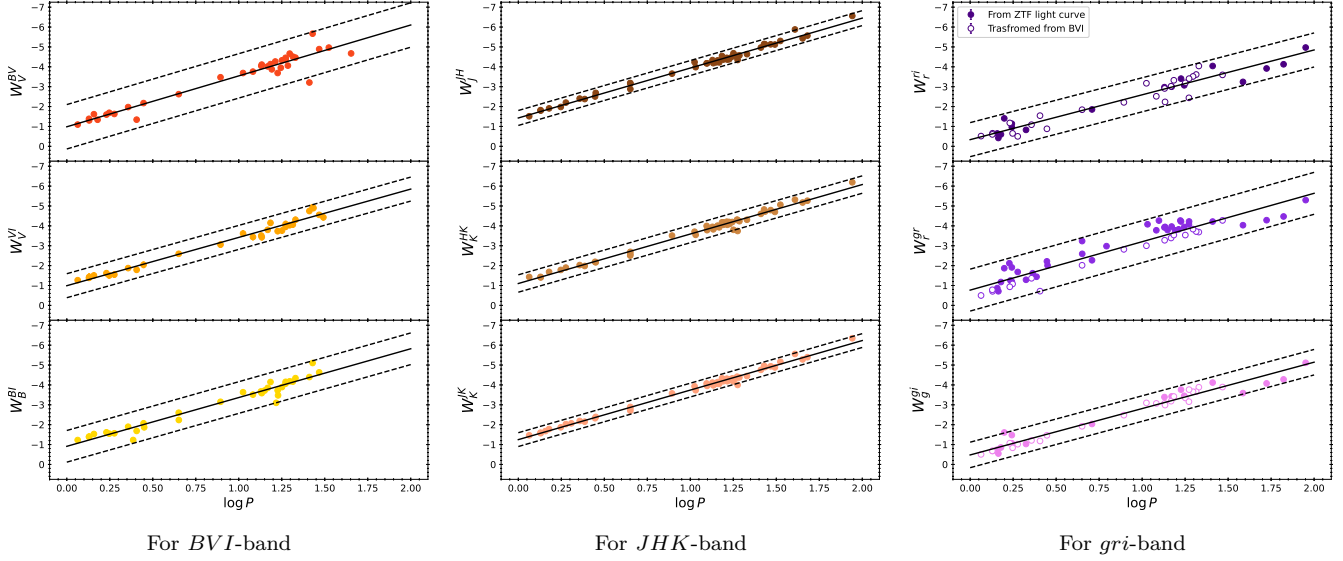


Figure 6. Same as Figure 4, but for the PW relations.

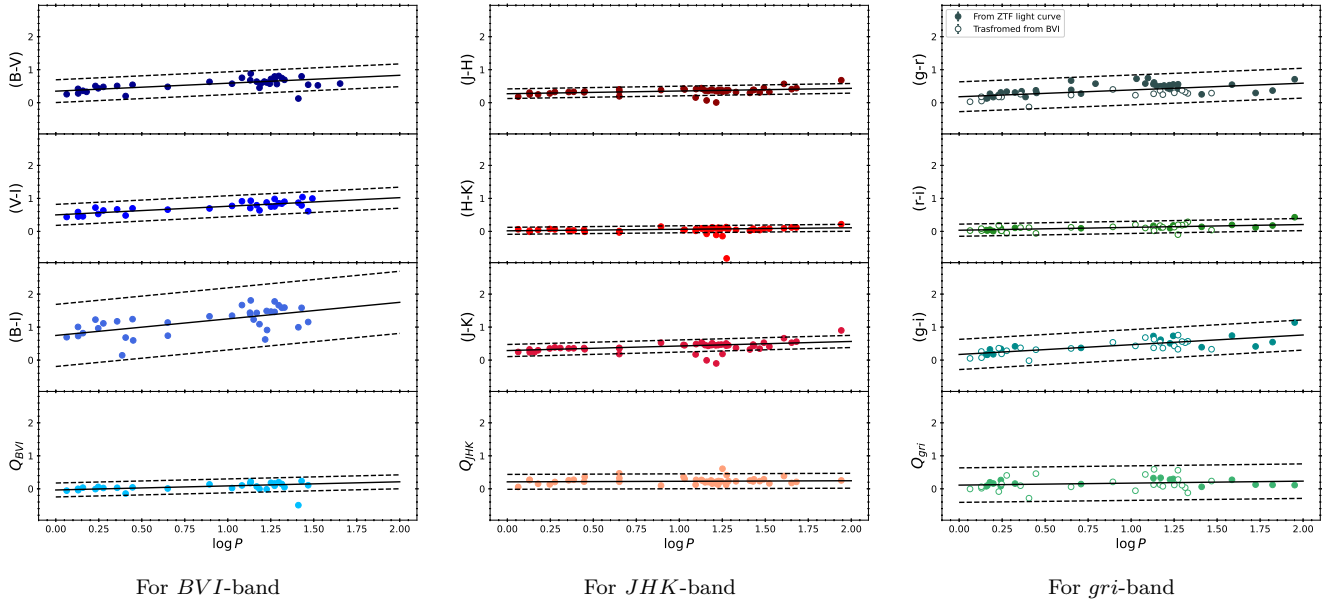


Figure 7. Same as Figure 4, but for the reddening-corrected PC relations (top three panels) and the reddening-free PQ relation (bottom panel). Scales on the y -axis were intended to be the same in all panels, such that the PC/PQ relations can be compared.

maintaining 272 THIC were plotted against their logarithmic period in the left panel of Figure 8, overlaid with the PC relations taken from Table 5. The $(r - i)$ colors for the M31 THIC are remarkable in good agreement with the $(r - i)$ PC relation derived from our sample of THIC located in the globular clusters. In contrast, outliers can be seen on the $(g - r)$ and $(g - i)$ PC relations, suggesting there could be some problems in the g -band. Indeed, the g -band observations were ~ 5 to ~ 10 times less than the ri -band (Kodric et al. 2018), such that the

g -band light curves do not have quality as good as in other two bands. As a result, out of the remaining 272 THIC, 50 of them do not have mean g -band magnitudes, and 161 of them carry a non-zero bit flag (see Table 2 of Kodric et al. 2018) indicating there are some problems associated with the g -band data. For these reasons, we only focused on the ri -band mean magnitudes for this sample of THIC in the subsequent analysis.

Right panels of Figure 8 present the ri -band PL/PW relations for the M31 THIC. We over-plotted the PL/PW

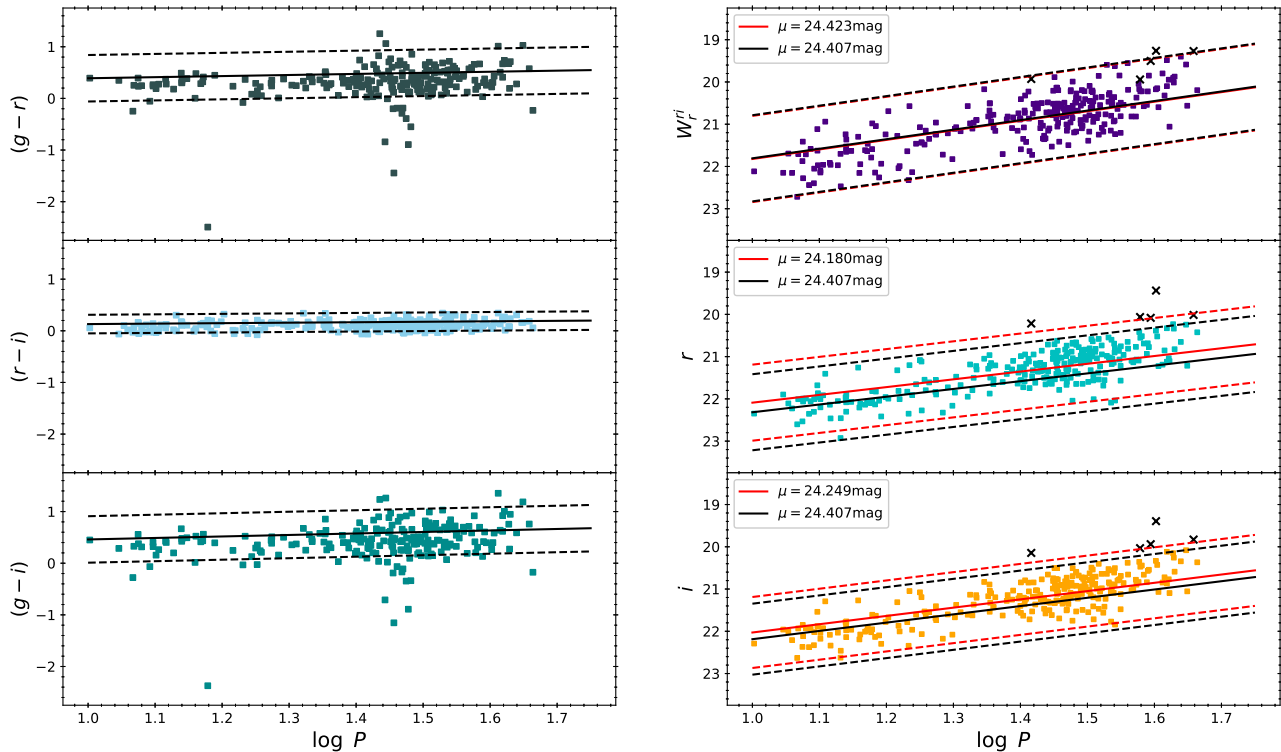


Figure 8. Left Panel: PC relations for the M31 TIIC, where the colors of the TIIC have been reddening-corrected (Kodric et al. 2018). The solid lines are the PC relations given in Table 5, together with the $\pm 3\sigma$ boundaries shown as dashed lines. **Right Panel:** The PW relation (top-right panel) for the W_r^{ri} Wesenheit-index, and the extinction-corrected ri -band PL relations (middle-right and bottom-right panels) for the M31 TIIC. Crosses represent the rejected TIIC as described in the text (see Section 6). Similar to the left panels, the solid lines are the PL/PW relations given in Table 3 and 4, respectively, shifted vertically with the distance modulus (μ) of M31, and the dashed lines are the corresponding $\pm 3\sigma$ boundaries. Black lines are the shifted PL/PW relations by adopting the same $\mu = 24.407$ mag (Li et al. 2021). The red lines represent the PL/PW relations after shifting the μ determined from fitting the data to the PL/PW relations given in Table 3 and 4. In both panels, error bars are omitted for clarity.

relations from Table 3 and 4, together with the respected $\pm 3\sigma$ boundaries, on the right panels of Figure 8 after shifting these PL/PW relations vertically with $\mu = 24.407$ mag (Li et al. 2021, as black lines). Except for five TIIC that appeared to be brighter (marked as crosses in the right panels of Figure 8) in the ri -band PL relations, almost all of the TIIC were confined within the $\pm 3\sigma$ of the respected PL/PW relations. Furthermore, scatters of these TIIC around the PL/PW relations confirmed the rather large dispersion in ri -band PL/PW relations as reported in Table 3 and 4.

Our derived PL/PW relations can also be used to determine the distance modulus of M31 from this sample of TIIC (after excluding the five TIIC marked as crosses in the right panels of Figure 8). By fitting the data with the ri -band PL/PW relations given in Table 3 and 4, weighted with the quadrature sums of errors on the mean magnitudes and the PL/PW dispersions, we obtained $\mu_r = 24.180 \pm 0.021$ mag, $\mu_i = 24.249 \pm 0.020$ mag, and $\mu_W = 24.423 \pm 0.026$ mag using the ri -band PL and PW relations, respectively. The quoted errors on μ are

statistical errors only. The μ_W obtained from fitting the PW relation is in good agreement, and lie in between, the measurement of $\mu = 24.407 \pm 0.032$ mag from Li et al. (2021) and the recommended value of $\mu = 24.46 \pm 0.10$ mag from de Grijs & Bono (2014). This suggested our derived ri -band PW relation is robust. On the other hand, distance moduli obtained from the ri -band PL relations are ~ 0.2 mag smaller than μ_W , hinting there could be additional systematic, in the order of ~ 0.2 mag, in the derived PL relations. Distances to the globular clusters adopted from Baumgardt & Vasiliev (2021) are unlikely to be the source of the systematic, because the same distances were used in deriving both of the PL and PW relations. Other possible systematic errors include the samples used, the extinction maps used, and the assumed extinction law to derive the ri -band PL relations.

The derivation of ri -band PL relations include the TIIC sample transformed from the BVI -band photometry. Therefore, we first excluded the TIIC with transformations and only using the TIIC that have ZTF ri -band

mean magnitudes, and re-derived the *ri*-band PL relations. Using the re-derived PL relations, the distance moduli of M31 we obtained are $\mu_r = 24.096 \pm 0.021$ mag and $\mu_i = 24.156 \pm 0.020$ mag. Similarly, we have used the “SFD” dust map for TIIC located outside the footprint of the *Bayerstar2019* reddening map. If we re-derived the *ri*-band PL relations by using the same “SFD” dust map to all TIIC in the sample and re-determined the distance moduli to M31, then we obtained $\mu_r = 24.000 \pm 0.021$ mag and $\mu_i = 24.115 \pm 0.020$ mag. Finally, we adopted the same extinction law as in [Kodric et al. \(2018\)](#), i.e. $A_r = 2.554E$ and $A_i = 1.893E$, and we obtained $\mu_r = 24.150 \pm 0.021$ mag and $\mu_i = 24.229 \pm 0.020$ mag. These distance moduli are smaller than those obtained from the *ri*-band PL relations derived in [Table 3](#). Hence, there could have hidden systematic errors when deriving the PL relations, and independent samples and calibration of the TIIC PL relations are desirable.

7. CONCLUSIONS

In this work, we present the first *gri*-band and the updated *BVIJHK*-band PL and PW relations for TIIC located in the globular clusters. All-together, there are 70 TIIC spanning in 30 globular clusters (with ages spanning from ~ 11.0 to ~ 13.2 Gyr) in our sample, and only three of them have the complete nine band photometry. Homogeneous distance to the globular clusters, ranging from 3.30 (M22) to 88.47 kpc (NGC2419), adopted from a single source ([Baumgardt & Vasiliev 2021](#)) and consistent reddening maps, either the *Bayerstar2019* 3D reddening map or the “SFD” dust map, were used to calibrate the absolute magnitudes of these samples of TIIC. We demonstrated that the PL relations are consistent in the *BVI* and the *gri* bands. We have also derived nine sets of the PW relations based on the combinations of these filters. For the PL/PW relations, the *JHK*-band PL/PW relations exhibit the smallest dispersion, which are preferable to be applied in the future distance scale work. Finally, our sample of TIIC also allow the derivation of PC and PQ relations in these filters. We found that the slopes of the PC relations in the *JHK*-band and in the $(r - i)$ color, as well as the slopes of the PQ relations, are quite shallow or flat.

We tested our PL/PW relations, at least in the *ri*-band, with a sizable sample of TIIC in M31. The scatters of M31 TIIC on the PL/PW relations are similar to those presented in [Table 3](#) and [4](#), confirming the derived PL/PW dispersions are intrinsic. Using our derived *ri*-band PW relation, the distance modulus of M31 we obtained is in agreement with the latest measurement using the classical Cepheids. However, distance moduli

derived from using the *ri*-band PL relations are smaller by ~ 0.2 mag, suggesting there could be hidden systematics in the derived PL relations. Therefore, additional work in the near future are required to independently crosscheck these PL relations. Nevertheless, our derived PW relations can be applied in the on-going and upcoming synoptic time-series sky surveys, such as LSST or other surveys employing similar *gri* filters.

ACKNOWLEDGMENTS

We are thankful for the useful discussions and comments from an anonymous referee that improved the manuscript. We are thankful for funding from the Ministry of Science and Technology (Taiwan) under the contracts 107-2119-M-008-014-MY2, 107-2119-M-008-012, 108-2628-M-007-005-RSP and 109-2112-M-008-014-MY3. AB acknowledges funding from the European Union’s Horizon 2020 research and innovation programme under the Marie Skłodowska-Curie grant agreement No. 886298.

Based on observations obtained with the Samuel Oschin Telescope 48-inch Telescope at the Palomar Observatory as part of the Zwicky Transient Facility project. ZTF is supported by the National Science Foundation under Grants No. AST-1440341 and AST-2034437 and a collaboration including current partners Caltech, IPAC, the Weizmann Institute of Science, the Oskar Klein Center at Stockholm University, the University of Maryland, Deutsches Elektronen-Synchrotron and Humboldt University, the TANGO Consortium of Taiwan, the University of Wisconsin at Milwaukee, Trinity College Dublin, Lawrence Livermore National Laboratories, IN2P3, University of Warwick, Ruhr University Bochum, Northwestern University and former partners the University of Washington, Los Alamos National Laboratories, and Lawrence Berkeley National Laboratories. Operations are conducted by COO, IPAC, and UW.

This research has made use of the SIMBAD database and the VizieR catalogue access tool, operated at CDS, Strasbourg, France. This research made use of Astropy,⁷ a community-developed core Python package for Astronomy ([Astropy Collaboration et al. 2013, 2018](#)).

Facility: PO:1.2m

Software: `astropy` ([Astropy Collaboration et al. 2013, 2018](#)), `dustmaps` ([Green 2018](#)), `gatspy`

⁷ <http://www.astropy.org>

(VanderPlas & Ivezić 2015), Matplotlib (Hunter 2007), NumPy (Harris et al. 2020), SciPy (Virtanen et al. 2020).

REFERENCES

- Alcock, C., Allsman, R. A., Alves, D. R., et al. 1998, *AJ*, 115, 1921
- Arellano Ferro, A., Luna, A., Bramich, D. M., et al. 2016, *Ap&SS*, 361, 175
- Arellano Ferro, A., Yezpez, M. A., Muneer, S., et al. 2020, *MNRAS*, 499, 4026
- Astropy Collaboration, Robitaille, T. P., Tollerud, E. J., et al. 2013, *A&A*, 558, A33
- Astropy Collaboration, Price-Whelan, A. M., Sipőcz, B. M., et al. 2018, *AJ*, 156, 123
- Baumgardt, H. & Vasiliev, E. 2021, *MNRAS*, 505, 5957
- Beaton, R. L., Bono, G., Braga, V. F., et al. 2018, *SSRv*, 214, 113
- Bellm, E. & Kulkarni, S. 2017, *Nature Astronomy*, 1, 0071
- Bellm, E. C., Kulkarni, S. R., Graham, M. J., et al. 2019, *PASP*, 131, 018002
- Berdnikov, L. N. & Pastukhova, E. N. 2021, *Astronomy Letters*, 47, 252
- Bhardwaj, A. 2020, *Journal of Astrophysics and Astronomy*, 41, 23
- Bhardwaj, A. 2022, *Universe*, 8, 122
- Bhardwaj, A., Rejkuba, M., Minniti, D., et al. 2017a, *A&A*, 605, A100
- Bhardwaj, A., Macri, L. M., Rejkuba, M., et al. 2017b, *AJ*, 153, 154
- Bhardwaj, A., Rejkuba, M., Sloan, G. C., et al. 2021, *ApJ*, 922, 20
- Bond, H. E., Ciardullo, R., & Siegel, M. H. 2016, *AJ*, 151, 40
- Braga, V. F., Bhardwaj, A., Contreras Ramos, R., et al. 2018, *A&A*, 619, A51
- Braga, V. F., Bono, G., Fiorentino, G., et al. 2020, *A&A*, 644, A95
- Breger, M. & Bregman, J. N. 1975, *ApJ*, 200, 343
- Ciechanowska, A., Pietrzyński, G., Szewczyk, O., et al. 2010, *Acta Astronomica*, 60, 233
- Chambers, K. C., Magnier, E. A., Metcalfe, N., et al. 2016, *arXiv:1612.05560*
- Clement, C. M. 2017, *yCat*, V/150
- Clement, C. C. & Hogg, H. S. 1978, *AJ*, 83, 167
- Clement, C. M., Sawyer Hogg, H., & Wells, T. R. 1980, *AJ*, 85, 1604
- Clement, C. M., Muzzin, A., Dufton, Q., et al. 2001, *AJ*, 122, 2587
- Contreras, R., Catelan, M., Smith, H. A., et al. 2010, *AJ*, 140, 1766
- Contreras Peña, C., Catelan, M., Grundahl, F., et al. 2018, *AJ*, 155, 116
- Corwin, T. M., Borissova, J., Stetson, P. B., et al. 2008, *AJ*, 135, 1459
- Das, S., Kanbur, S. M., Smolec, R., et al. 2021, *MNRAS*, 501, 875
- Deb, S. & Singh, H. P. 2009, *A&A*, 507, 1729
- de Grijs, R. & Bono, G. 2014, *AJ*, 148, 17
- Dekany, R., Smith, R. M., Riddle, R., et al. 2020, *PASP*, 132, 038001
- Demers, S. 1969, *AJ*, 74, 925
- Demers, S. & Wehlau, A. 1971, *AJ*, 76, 916
- Demers, S. & Harris, W. E. 1974, *AJ*, 79, 627
- Dias, B., Barbuy, B., Saviane, I., et al. 2015, *A&A*, 573, A13
- Dias, B., Barbuy, B., Saviane, I., et al. 2016a, *A&A*, 590, A9
- Dias, B., Saviane, I., Barbuy, B., et al. 2016b, *The Messenger*, 165, 19
- Di Criscienzo, M., Caputo, F., Marconi, M., et al. 2007, *A&A*, 471, 893
- Graham, M. J., Kulkarni, S. R., Bellm, E. C., et al. 2019, *PASP*, 131, 078001
- Green, G. M. 2018, *The Journal of Open Source Software*, 3, 695
- Green, G. M., Schlafly, E., Zucker, C., et al. 2019, *ApJ*, 887, 93
- Groenewegen, M. A. T., Udalski, A., & Bono, G. 2008, *A&A*, 481, 441
- Groenewegen, M. A. T. & Jurkovic, M. I. 2017, *A&A*, 604, A29
- Harris, C. R., Millman, K. J., van der Walt, S. J., et al. 2020, *Nature*, 585, 357
- Hazen-Liller, M. L. 1985, *AJ*, 90, 1807
- Hunter, J. D. 2007, *Computing in Science and Engineering*, 9, 90
- Ivezić, Ž., Kahn, S. M., Tyson, J. A., et al. 2019, *ApJ*, 873, 111
- Johnson, H. L. & Morgan, W. W. 1953, *ApJ*, 117, 313
- Karmakar, P., Smith, H. A., & De Lee, N. 2019, *JAAVSO*, 47, 167
- Kodric, M., Riffeser, A., Hopp, U., et al. 2018, *AJ*, 156, 130
- Kopacki, G. 2013, *Acta Astronomica*, 63, 91
- Kubiak, M. & Udalski, A. 2003, *Acta Astronomica*, 53, 117

- Kunder, A., Stetson, P. B., Catelan, M., et al. 2013, *AJ*, 145, 33
- Li, S., Riess, A. G., Busch, M. P., et al. 2021, *ApJ*, 920, 84
- Madore, B. F. 1982, *ApJ*, 253, 575
- Madore, B. F. & Freedman, W. L. 1991, *PASP*, 103, 933
- Magnier, E. A., Sweeney, W. E., Chambers, K. C., et al. 2020, *ApJS*, 251, 5
- Masci, F. J., Laher, R. R., Rusholme, B., et al. 2019, *PASP*, 131, 018003
- Matsunaga, N., Fukushi, H., Nakada, Y., et al. 2006, *MNRAS*, 370, 1979
- Matsunaga, N., Feast, M. W., & Menzies, J. W. 2009, *MNRAS*, 397, 933
- Matsunaga, N., Feast, M. W., & Soszyński, I. 2011, *MNRAS*, 413, 223
- Nemec, J. M., Nemec, A. F. L., & Lutz, T. E. 1994, *AJ*, 108, 222
- Ngeow, C.-C., Liao, S.-H., Bellm, E. C., et al. 2021, *AJ*, 162, 63
- Ngeow, C.-C., Bhardwaj, A., Dekany, R. et al. 2022, *AJ*, 163, 239
- Osborn, W., Kopacki, G., & Haberstroh, J. 2012, *Acta Astronomica*, 62, 377
- Osborn, W., Kopacki, G., Smith, H. A., et al. 2019, *Acta Astronomica*, 69, 101
- Percy, J. R., Bezuhly, M., Milanowski, M., et al. 1997, *PASP*, 109, 264
- Percy, J. R. & Hoss, J. X. 2000, *JAAVSO*, 29, 14
- Plachy, E., Molnár, L., Jurkovic, M. I., et al. 2017, *MNRAS*, 465, 173
- Prieto, G., Catelan, M., Contreras Ramos, R., et al. 2012, *A&A*, 543, A148
- Pritzl, B. J., Smith, H. A., Stetson, P. B., et al. 2003, *AJ*, 126, 1381
- Rabidoux, K., Smith, H. A., Pritzl, B. J., et al. 2010, *AJ*, 139, 2300
- Ripepi, V., Moretti, M. I., Marconi, M., et al. 2015, *MNRAS*, 446, 3034
- Ripepi, V., Molinaro, R., Musella, I., et al. 2019, *A&A*, 625, A14
- Ripepi, V., Clementini, G., Molinaro, R., et al. 2022, *arXiv:2206.06212*
- Rozyczka, M., Thompson, I. B., Pych, W., et al. 2017, *Acta Astronomica*, 67, 203
- Rozyczka, M., Narloch, W., Schwarzenberg-Czerny, A., et al. 2018, *Acta Astronomica*, 68, 237
- Sandage, A. & Tammann, G. A. 2006, *ARA&A*, 44, 93
- Schlafly, E. F. & Finkbeiner, D. P. 2011, *ApJ*, 737, 103
- Schlegel, D. J., Finkbeiner, D. P., & Davis, M. 1998, *ApJ*, 500, 525
- Schmidt, E. G., Johnston, D., Langan, S., et al. 2004, *AJ*, 128, 1748
- Schmidt, E. G., Johnston, D., Langan, S., et al. 2005a, *AJ*, 129, 2007
- Schmidt, E. G., Johnston, D., Langan, S., et al. 2005b, *AJ*, 130, 832
- Skottfelt, J., Bramich, D. M., Figuera Jaimes, R., et al. 2015, *A&A*, 573, A103
- Skrutskie, M. F., Cutri, R. M., Stiening, R., et al. 2006, *AJ*, 131, 1163
- Soszyński, I., Udalski, A., Szymański, M. K., et al. 2018, *Acta Astronomica*, 68, 89
- Tonry, J. L., Stubbs, C. W., Lykke, K. R., et al. 2012, *ApJ*, 750, 99
- Udalski, A., Soszyński, I., Pietrukowicz, P., et al. 2018, *Acta Astronomica*, 68, 315
- VanderPlas, J. T., & Ivezić, Ž. 2015, *ApJ*, 812, 18
- VanderPlas, J. 2016, *gatspy: General tools for Astronomical Time Series in Python*, ascl:1610.007
- Vásquez, S., Saviane, I., Held, E. V., et al. 2018, *A&A*, 619, A13
- Virtanen, P., Gommers, R., Oliphant, T. E., et al. 2020, *Nature Methods*, 17, 261
- Wallerstein, G. 2002, *PASP*, 114, 689
- Wehlau, A. & Bohlender, D. 1982, *AJ*, 87, 780
- Wehlau, A. & Hogg, H. S. 1985, *AJ*, 90, 2514
- Wehlau, A. & Butterworth, S. 1990, *AJ*, 100, 686
- Wehlau, A., Hogg, H. S., & Butterworth, S. 1990, *AJ*, 99, 1159
- Welch, D. L. 2012, *JAAVSO*, 40, 492
- Wielgórski, P., Pietrzyński, G., Pilecki, B., et al. 2022, *ApJ*, 927, 89
- Yepez, M. A., Arellano Ferro, A., Deras, D., et al. 2022, *MNRAS*, 511, 1285